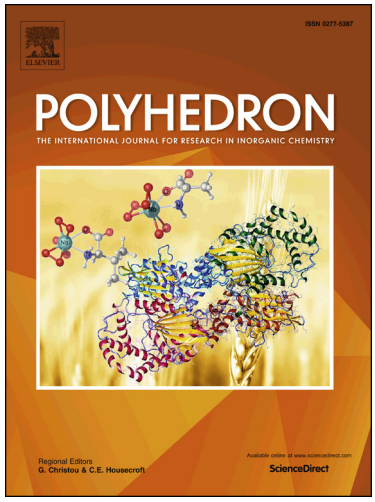

Electrocatalytic proton reduction by $[Fe(CO)_2(\kappa^2\text{-dppv})(\kappa^1\text{-SAr})_2]$ (dppv = *cis*-1,2-bis(diphenylphosphino)ethylene; Ar = C_6F_5, C_6H_5, $C_6H_4CH_3$-*p*)

Shishir Ghosh, Nathan Hollingsworth, Mark Warren, Katherine B. Holt, Graeme Hogarth

PII: S0277-5387(17)30529-6
DOI: http://dx.doi.org/10.1016/j.poly.2017.08.008
Reference: POLY 12772

To appear in: *Polyhedron*

Received Date: 16 June 2017
Revised Date: 4 August 2017
Accepted Date: 7 August 2017

Please cite this article as: S. Ghosh, N. Hollingsworth, M. Warren, K.B. Holt, G. Hogarth, Electrocatalytic proton reduction by $[Fe(CO)_2(\kappa^2\text{-dppv})(\kappa^1\text{-SAr})_2]$ (dppv = *cis*-1,2-bis(diphenylphosphino)ethylene; Ar = C_6F_5, C_6H_5, $C_6H_4CH_3$-*p*), *Polyhedron* (2017), doi: http://dx.doi.org/10.1016/j.poly.2017.08.008

Electrocatalytic proton reduction by $[Fe(CO)_2(\kappa^2\text{-dppv})(\kappa^1\text{-SAr})_2]$ (dppv = *cis*-1,2-bis(diphenylphosphino)ethylene; Ar = C_6F_5, C_6H_5, $C_6H_4CH_3$-*p*)

Shishir Ghosh[a,b,*], Nathan Hollingsworth[a], Mark Warren[c], Katherine B. Holt[a], Graeme Hogarth[d,*]

[a] *Department of Chemistry, University College London, 20 Gordon Street, London WC1H OAJ, UK*

[b] *Department of Chemistry, Jahangirnagar University, Savar, Dhaka 1342, Bangladesh*

[c] *Diamond Light Source, Harwell Science and Innovation Campus, Didcot, Oxfordshire OX11 0DE, UK*

[d] *Department of Chemistry, King's College London, Britannia House, 7 Trinity Street, London SE1 1DB, UK*

*Corresponding authors. E-mail addresses: sghosh_006@yahoo.com (S. Ghosh), graeme.hogarth@kcl.ac.uk (G. Hogarth)

ABSTRACT

Electrocatalytic reduction of protons to hydrogen by mononuclear iron complexes which are developed as models of the distal iron center of [FeFe]-hydrogenase active site are described. A series of iron(II) bis(thiolate) complexes $[Fe(CO)_2(\kappa^2\text{-dppv})(\kappa^1\text{-SAr})_2]$ (**1**, Ar = C_6F_5; **2**, Ar = C_6H_4; **3**, Ar = $C_6H_4CH_3$-*p*; dppv = *cis*-1,2-bis(diphenylphosphino)ethylene) have been prepared from direct reactions between the corresponding hexacarbonyl $[Fe_2(CO)_6(\mu\text{-SAr})_2]$ and dppv at elevated temperatures. Structurally they are similar being coordinated by a chelating dppv, two carbonyls and two thiolato ligands bonded in an all *cis*-arrangement. Solution spectroscopic data indicate that they exist in two isomeric forms in solution. All reversibly protonate at sulphur atom(s) upon addition of $HBF_4{\cdot}Et_2O$ and lose a thiolate ligand as thiol. They show a common quasi-reversible reductive feature (attributed to the Fe^{II}/Fe^{I} couple) in their CVs in addition to other redox responses and are able to catalyze reduction of protons to hydrogen at their Fe(I) oxidation state in presence of $HBF_4{\cdot}Et_2O$. Complex **1** is the

most efficient catalyst and catalyzes proton reduction at *ca.* –1.5 V showing $i_{cat}/i_p \geq 46$ in the presence of ten equivalents of $HBF_4 \cdot Et_2O$.

Keywords**:** Iron(II) complexes; Thiolate; Diphosphine; Hydrogenase biomimics; Electrocatalysis

Introduction

Hydrogenases (H_2ases) catalyse the reversible inter-conversion of protons and hydrogen [1,2], a reaction of great importance in developing a carbon-neutral economy, and consequently significant efforts have been made to develop cheap and robust catalysts which can mimic the function of H_2ases [2,3]. The active site of [FeFe]-H_2ases consists of a diiron core bound to a cysteine-linked $[Fe_4S_4]$ cluster, and supported by CO and cyanide ligands and a bridging azadithiolate (SCH_2NHCH_2S) group [4]. This has lead researchers to investigate a large number of dithiolate-bridged diiron complexes as structural and functional models of the [FeFe]-H_2ases [2,3]. Catalytic pathways involved in H_2 production and oxidation have recently been delineated [5]; for proton reduction, proton binding and hydride-proton combination leading to hydrogen evolution occur at the distal centre (Fe_d in Chart 1a), the proximal iron (Fe_p in Chart 1a) acting as a channel for electron-transfer between the distal centre and $[Fe_4S_4]$ cluster. This suggests then that mononuclear iron complexes which possess a close structural resemblance with the distal iron centre may catalyze proton reduction as electrons can be delivered directly from an electrode. However, in comparison to the efforts directed toward diiron complexes, relatively little attention has been paid to mononuclear iron complexes [6-15] even though the iron-porphyrin complex, [(TPP)Fe(Cl)] (TPP = tetraphenylporphyrin), was shown to catalyse proton reduction in 1996 [6]. More recently, proton reduction by a number of mononuclear iron complexes has been reported [7-15]; for example, Winkler and co-workers explored fluorinated diglyoxime-iron complexes [7], Artero and Fontecave utilised a cyclopentadienyl complex [8] and an iron polypyridyl complex was found to catalyse H_2 formation from aqueous solutions with turnover frequencies of up to 3000 s^{-1} [13]. The catalytic pathway(s) for all of these electronically saturated catalysts is proposed to involve loss of a coordinated ligand upon reduction thus creating a vacant coordination site which can accommodate the incoming proton(s) [7,8]. In contrast, mononuclear iron catalysts developed by Ott and co-workers (Chart 1b) [9], that

have a close structural resemblance to Fe_d of the active site of [FeFe]-H_2ases operate in a different fashion. These octahedral complexes undergo reversible protonation at sulphur and show two catalytic waves with different turnover rates, indicating that H_2 production occurs *via* two pathways [9]. Theoretical studies support a mechanism in which protonation at sulphur followed by an one-electron reduction results in Fe–S bond scission to form a penta-coordinated iron(II) intermediate (Scheme 1). The latter either protonates at the metal centre and then undergoes subsequent reduction at the same potential, or reduces at a more negative potential followed by protonation at metal centre to give a neutral hydride species. Interaction between the basic iron-bound hydride and the acidic sulphur-bound proton leads to the formation of H_2, regenerating the catalyst. Since a vacant coordination site is necessary to reduce protons at the iron centre, a number of square-pyramidal 16-electron iron complexes have also been tested by Ott [10,11] and Jones [12].

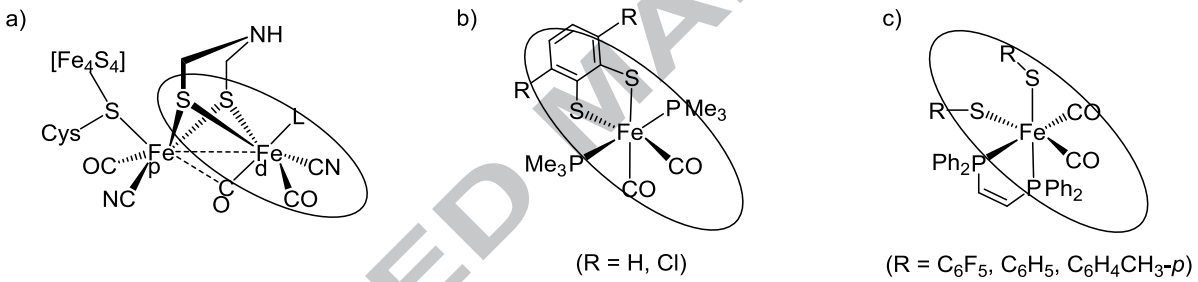

Chart 1. (a) The active site of the [FeFe]-H_2ase, (b) model complexes studied by Ott [9] and (c) model complexes studied by us (presented in this work). Structural similarities between the distal iron centre and the model complexes are highlighted.

In a recent contribution, we detailed the electrocatalytic proton reduction catalysed by the perfluorinated diiron bis(thiolate) complex, $[Fe_2(CO)_6(\mu\text{-}SC_6F_5)_2]$ [16]. Experiments showed that the *in-situ* generated radical anion, $[Fe_2(CO)_6(\mu\text{-}SC_6F_5)_2]^-$, has limited stability in the absence of CO and partially decomposes into mononuclear species, the latter showing significantly better catalytic activity than the initial diiron complex. This observation prompted us to investigate the proton reduction ability of the related mononuclear iron complex, $[Fe(CO)_2(\kappa^2\text{-dppv})(\kappa^1\text{-}SC_6F_5)_2]$ (**1**). Herein we report that **1** exhibits high catalytic activity towards proton reduction at *ca.* –1.5 V *vs.* Fc^+/Fc with an impressive i_{cat}/i_p ratio of 46 after addition of just 10 equivalents of $HBF_4{\cdot}Et_2O$. For comparison, the proton reduction ability of the analogous phenyl- and *p*-tolyl-thiolate complexes $[Fe(CO)_2(\kappa^2\text{-dppv})(\kappa^1\text{-}SC_6H_5)_2]$ (**2**) and $[Fe(CO)_2(\kappa^2\text{-dppv})(\kappa^1\text{-}SC_6H_4CH_3\text{-}p)_2]$ (**3**) is also reported.

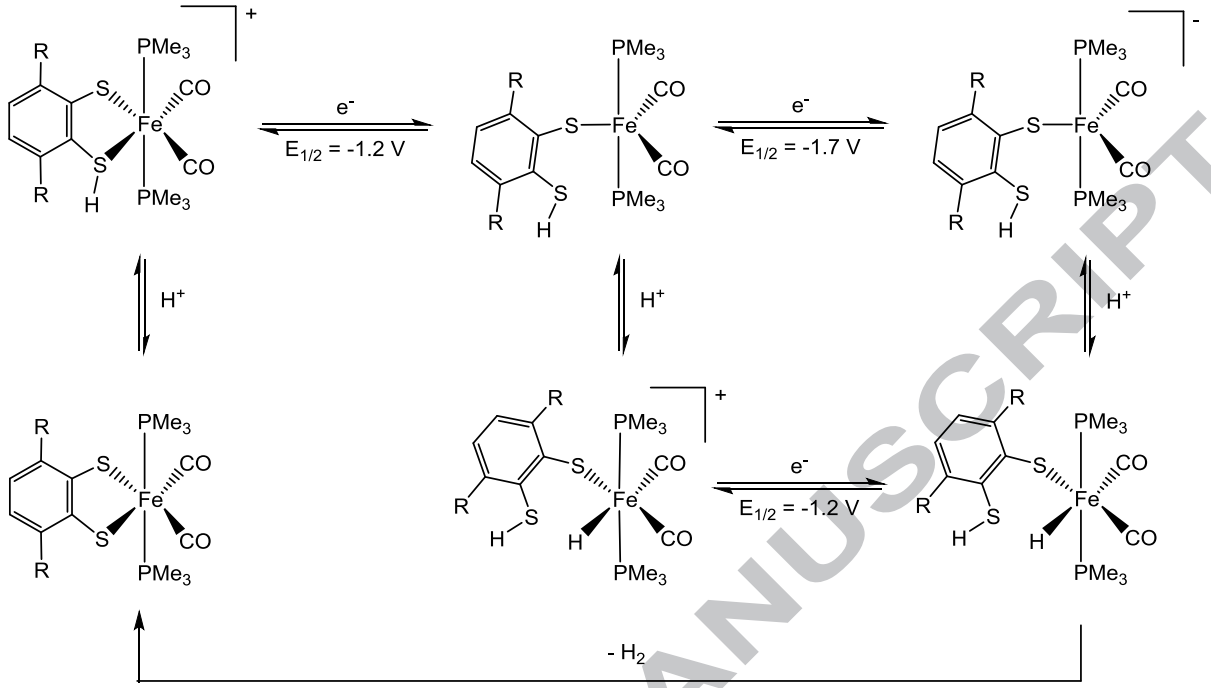

Scheme 1. Catalytic mechanism proposed for [Fe(CO)$_2$(PMe$_3$)$_2$(κ^2-SC$_6$H$_2$R$_2$S)] (R = H, Cl) [9].

Results and discussion

Synthesis and characterisation

Complexes **1**-**3** were synthesized from reactions of [Fe$_2$(CO)$_6$(μ-SAr)$_2$] and dppv at elevated temperatures (Scheme 2), following the method reported by Haines. [17]. Complexes of the general formula [Fe(CO)$_2$(κ^2-diphosphine)(κ^1-SAr)$_2$] can also be synthesized from Fe^{2+} salts by treatment with CO in the presence of diphosphine and ArS$^-$ as reported by Markó. [18]. All of them are air-stable in solid-state but decompose in organic solutions when exposed to air. Air stability in solution decreases with increasing electron-donating ability of the thiolate, with **1** being the most stable.

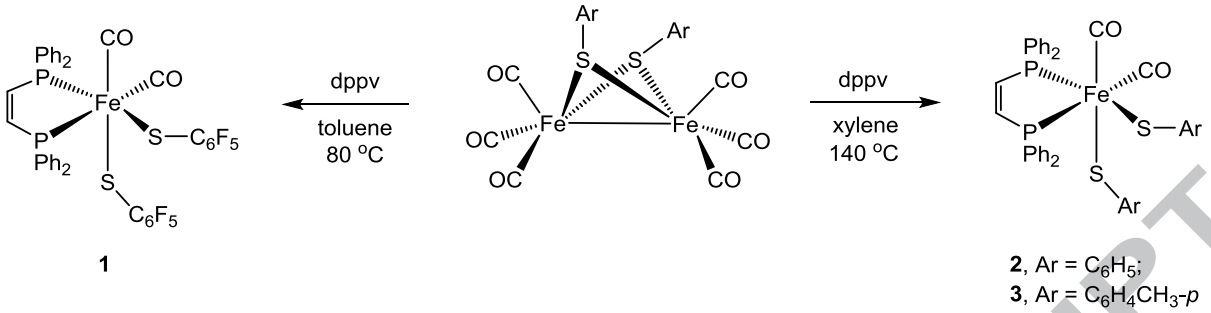

Scheme 2. Synthesis of $[Fe(CO)_2(\kappa^2\text{-dppv})(\kappa^1\text{-SAr})_2]$ complexes (**1**-**3**).

IR spectra of **1-3** show two strong absorption bands in the carbonyl stretching region indicating that the carbonyl ligands are in *cis*-orientation, which is also confirmed by X-ray crystallography (see later). The $^{31}P\{^1H\}$ NMR spectra indicate the presence of two isomers in solution, with each showing a pair of doublets and a singlet (Fig. S1). Three isomers are possible for this type of complex (Chart 2). The major isomer is 'all-*cis*' in which the two phosphorus atoms are non-equivalent and this is responsible for the appearance of the doublets in the $^{31}P\{^1H\}$ NMR spectra. In both 'S-*trans*' and 'CO-*trans*' the phosphorus atoms are equivalent, thus one should expect a singlet in the $^{31}P\{^1H\}$ NMR spectrum for both. We assume that the minor isomer is the 'S-*trans*' configuration, as 'CO-*trans*' is electronically less favourable since the two strong π-acid ligands (carbonyls) are in a *trans*-orientation. The amount of the minor isomer increases with the electron-donating ability of the thiolate, the major/minor ratio being 20:1, 13:1 and 4:1 for **1**, **2** and **3**, respectively. Variable temperature NMR studies of **1** and **3** (in CD_2Cl_2 between +40 to -40 °C) show that the isomeric ratio does not change with temperature.

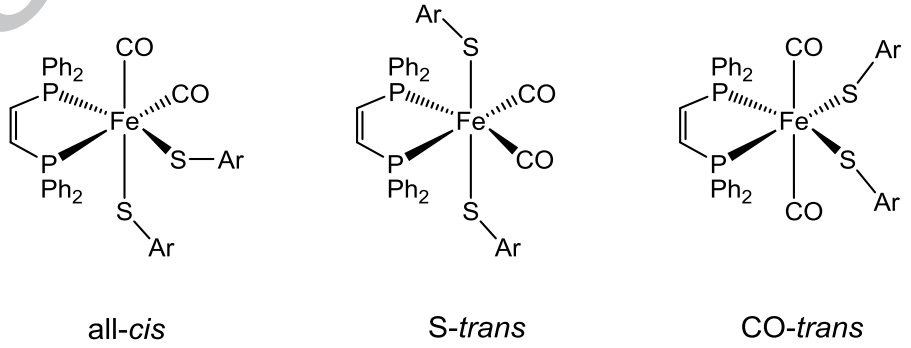

Chart 2. Possible isomers of $[Fe(CO)_2(\kappa^2\text{-dppv})(\kappa^1\text{-SAr})_2]$.

The solid-state structures of **1-3** are similar and all adopt 'all-*cis*' (Chart 2) isomeric form, which is also the predominant species in solution. Unfortunately disorders associated with

residual solvent in **1** and the phenyl rings of the thiolate ligands in **2** lead to poor overall structural models which preclude a detailed discussion of structural parameters. Nevertheless, the structures provide sufficient information about the geometry of the molecule and the orientation of the ligands and are shown in Figs. S2 and S3. In both, the iron adopts a distorted octahedral geometry with the carbonyls and thiolate ligands in mutually *cis*-orientations. We obtained better quality crystals of **3**, the structure of which is shown in Fig. 1, with the caption containing selected bond lengths and angles. Both the carbonyls and the thiolate ligands adopt *cis*-configuration. The coordination geometry around iron can be best described as a distorted octahedron, which is evident from the reduction of P–Fe–P chelate angle and expansion of the S–Fe–S angle to 86.33(2)° and 94.03(2)° respectively. The Fe–CO bond distance *trans* to the thiolate ligand [Fe(1)–C(1) 1.776(2) Å] is slightly shorter than that *trans* to phosphine Fe(1)–C(11) 1.798(3) Å], while both Fe–P and Fe–S distances are similar to those in related complexes [18].

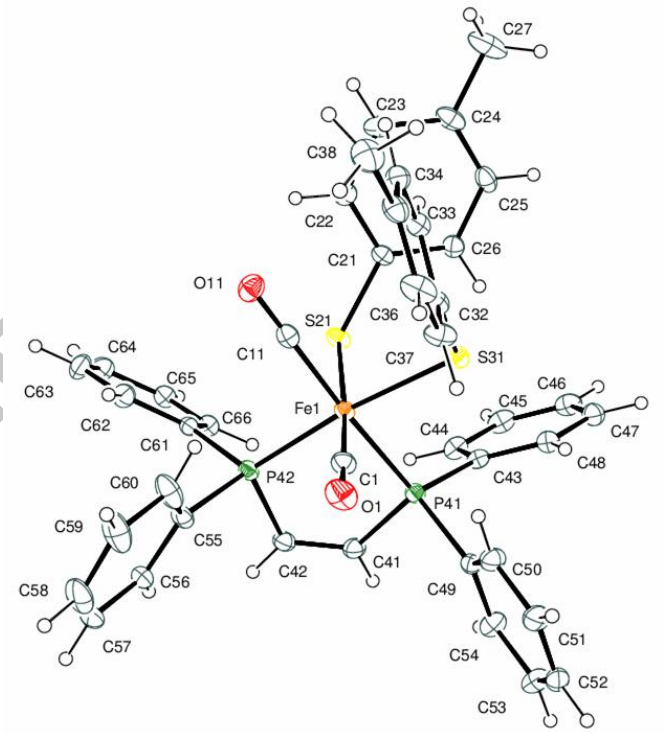

Fig. 1. An ORTEP diagram of the molecular structure of $[Fe(CO)_2(\kappa^2\text{-dppv})(\kappa^1\text{-}SC_6H_4CH_3\text{-}p)_2]$ (**3**) showing 50% thermal ellipsoids. Selected bond lengths (Å) and angles(°): Fe(1)–C(1) 1.776(2), Fe(1)–C(11) 1.798(3), Fe(1)–P(41) 2.2756(7), Fe(1)–P(42) 2.2415(6), Fe(1)–S(21) 2.3722(5), Fe(1)–S(31) 2.3547(6), P(41)–Fe(1)–P(42) 86.33(2), S(21)–Fe(1)–S(31) 94.03(2), C(1)–Fe(1)–C(11) 93.60(10), C(1)–Fe(1)–P(41) 94.17(8), S(21)–Fe(1)–P(42) 85.58(2), S(21)–Fe(1)–C(1) 174.94(8), S(31)–Fe(1)–P(42) 172.68(3), C(11)–Fe(1)–P(41) 172.21(6).

Reactions with acid

We next assessed the proton-binding ability of **1**-**3**, since the coordination of the proton(s) at the active centre of a catalyst is a key step in the electrocatalytic conversion of protons to hydrogen. The reactions of **1**-**3** with acid were carried out using $HBF_4{\cdot}Et_2O$. Addition of $HBF_4{\cdot}Et_2O$ to a CH_2Cl_2 solution of **1** at room temperature resulted in a colour change from red to yellow, absorptions at 2037 and 1993 cm^{-1} for the neutral complex being replaced by new features at 2062 and 2017 cm^{-1} attributed to $\mathbf{1H}^+$ (Fig. 2 and Scheme 3). The small blue shift (25 cm^{-1}) of the highest energy absorption points towards protonation at sulphur [9]. Protonation of **1** is reversible as the original IR spectrum was recovered upon immediate addition of PPh_3 to the protonated solution. However, in the absence of PPh_3 over a few minutes bands associated with $\mathbf{1H}^+$ diminish with concomitant appearance of new absorptions at 2100, 2064 and 2024 cm^{-1} suggesting further structural change. The 63 cm^{-1} blue shift of the highest energy absorption suggests that the iron loses significant electron-density during the process. We propose that after protonation at sulphur a penta-coordinated cationic species, $(\mathbf{1'})^+$, may form upon loss of C_6F_5SH from $\mathbf{1H}^+$ (Scheme 3). As trigonal bipyramidal complexes are generally highly fluxional, the resultant species may adopt different isomeric forms in solution. As far as we are aware, there is no precedence of such cationic penta-coordinated species of iron.

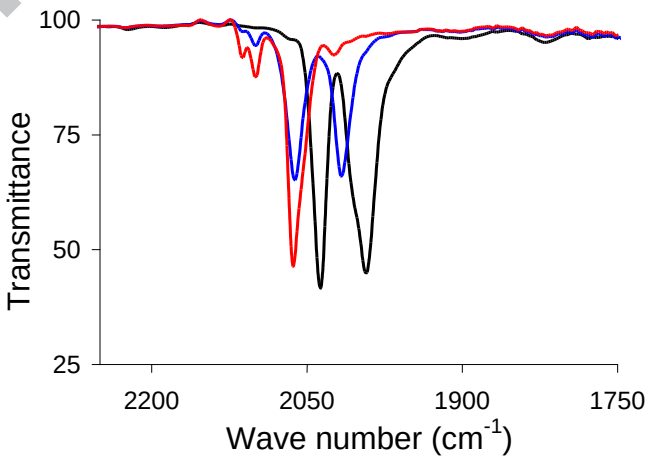

Fig. 2. IR spectrum of $[Fe(CO)_2(\kappa^2\text{-dppv})(\kappa^1\text{-}SC_6F_5)_2]$ (**1**) in CH_2Cl_2 – in absence of acid (**1**, black), after addition of 2 equiv. of $HBF_4{\cdot}Et_2O$ ($\mathbf{1H}^+$, blue), after 5 min of acid addition $[(\mathbf{1'})^+$, red].

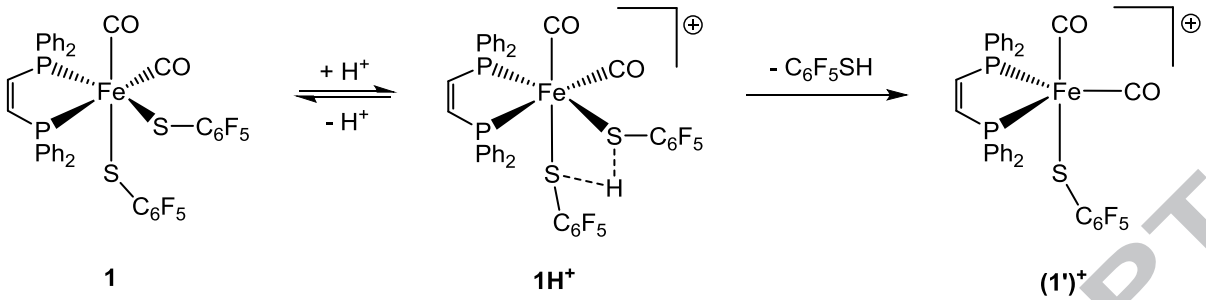

Scheme 3. Proposed protonation chemistry of $[Fe(CO)_2(\kappa^2\text{-dppv})(\kappa^1\text{-}SC_6F_5)_2]$ (**1**)

Protonation of **2** is also accompanied by a colour change from red to yellow with the replacement of the absorptions at 2023 and 1978 cm^{-1} (for **2**) by three new absorptions at 2092, 2056 and 2019 cm^{-1} (Fig. 3). In this case, we have not seen the absorption bands for $\mathbf{2H^+}$ which suggests that it is relatively unstable and loses C_6H_5SH after protonation much faster than $\mathbf{1H^+}$ loses C_6F_5SH. Similar results were observed upon addition of $HBF_4{\cdot}Et_2O$ to CH_2Cl_2 solution of **3**; absorptions at 2020 and 1975 cm^{-1} were replaced by a new set at 2058, 2016 and 1990 cm^{-1}. Attempts to monitor protonation of these complexes *via* NMR spectroscopy were unsuccessful which we assume is due to the fluxionality and instability of the resulted penta-coordinated cationic species.

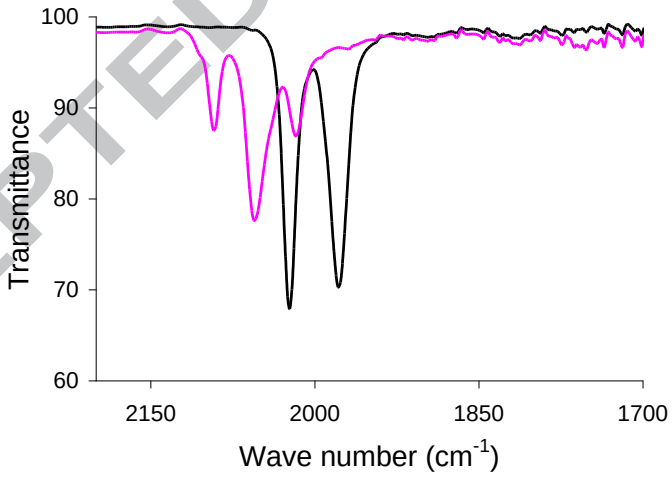

Fig. 3. IR spectrum of $[Fe(CO)_2(\kappa^2\text{-dppv})(\kappa^1\text{-}SC_6H_5)_2]$ (**2**) in CH_2Cl_2 – in absence of acid (black) and after addition of 2 equiv. of $HBF_4{\cdot}Et_2O$ (pink).

Electrochemistry and catalysis

In order to asses the proton reduction ability of **1-3**, CVs were recorded in MeCN in the absence and in the presence of various concentration of $HBF_4{\cdot}Et_2O$. In the absence of acid, **1** shows a

quasi-reversible reduction at $E_{1/2}$ = –1.43 V (Fig. 4a) the reversibility of which does not improve as the scan rate is varied followed by an irreversible reduction at E_p = 2.45 V. Complex **1** also exhibits an oxidation at E_p = 0.80 V which shows some reversibility at slow scan rates (≤ 0.5 V/s). Upon addition of one equivalent of $HBF_4{\cdot}Et_2O$, the CV now shows three new reduction peaks at E_p = –0.95, –1.35 V and –1.95 V (Fig. 4b), the first reduction showing a *ca.* 0.5 V positive shift upon protonation. The peak current of this peak did not increase with increasing acid concentration but those of the second and third waves increased sequentially upon addition of acid being characteristic of proton reduction (Fig. 4c). After addition of *ca.* ten equivalents of acid the peak potential (E_p) of the second wave shifted to *ca.* –1.6 V and the i_{cat}/i_p ratio is estimated at 46. The third reduction wave shifts to –2.20 V (a negative shift of –0.25 V) upon addition of two equivalents of acid and the peak height of this wave increases gradually with the acid concentration, showing an i_{cat}/i_p ratio of 27 after addition of ten equivalents of acid. Usually for mononuclear catalysts, the observation of two catalytic waves with distinct peak currents indicates production of hydrogen *via* two pathways [9] with the catalyst being more efficient at more negative potentials. But in the case of **1**, the catalyst shows better efficiency at the second reduction wave as compared to that at the third. Taking account of this, together with the –0.25 V negative shift of the third reduction wave upon addition of two equivalents of acid, we suggest that **1** degrades to some unidentified species which is responsible for catalysis at the third reduction wave.

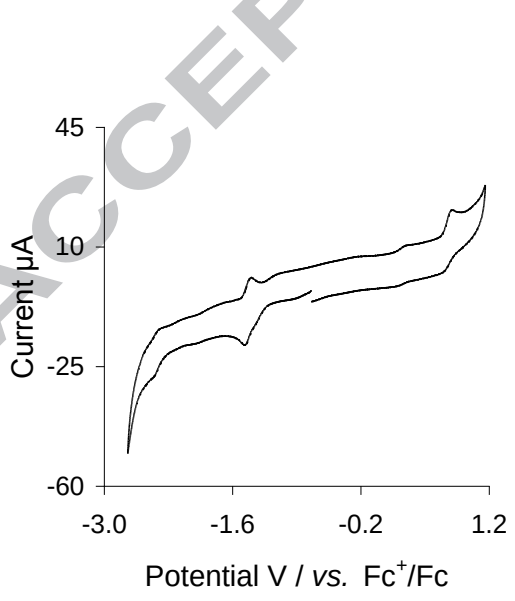

(a)

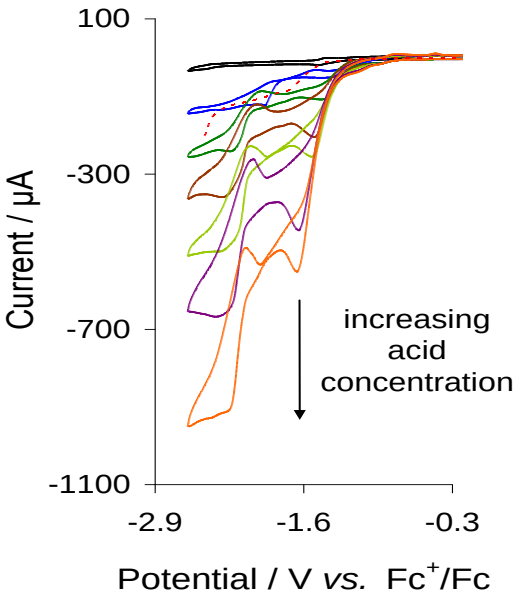

(b)

Fig. 4 (a) CV of **1**; (b) CVs of **1** in the absence of acid (black) and in the presence of 1 (blue), 3 (green), 5 (brown), 6 (lime), 8 (violet) and 9 (orange) equivalents of $HBF_4{\cdot}Et_2O$ (0.5 m*M* solution in MeCN, supporting electrolyte $[NBu_4][PF_6]$, scan rate 0.1 Vs^{-1}, glassy carbon electrode, potential vs Fc^+/Fc). Response of 20 equivalents $HBF_4{\cdot}Et_2O$ alone is shown with the red dotted line.

A speculative pathway for electrocatalytic proton reduction by **1** is shown in Scheme 4. The first step is the reversible protonation at sulphur to give $\mathbf{1H}^+$ followed by reduction at E_p = –0.95 V, the latter being accompanied by loss of thiol to form **1′** [9]. This 17-electron penta-coordinated species has a vacant coordination site but may not be basic enough to bind a proton. It therefore undergoes a second reduction (at E_p = –1.35 V) to give $(\mathbf{1'})^-$ which can either protonate, to form **1′H**, or undergo a further reduction at E_p = –2.20 V, **1′H** releasing hydrogen *via* homolytic (bimolecular reaction) and/or heterolytic pathways to regenerate **1′** thereby completing the catalytic cycle.

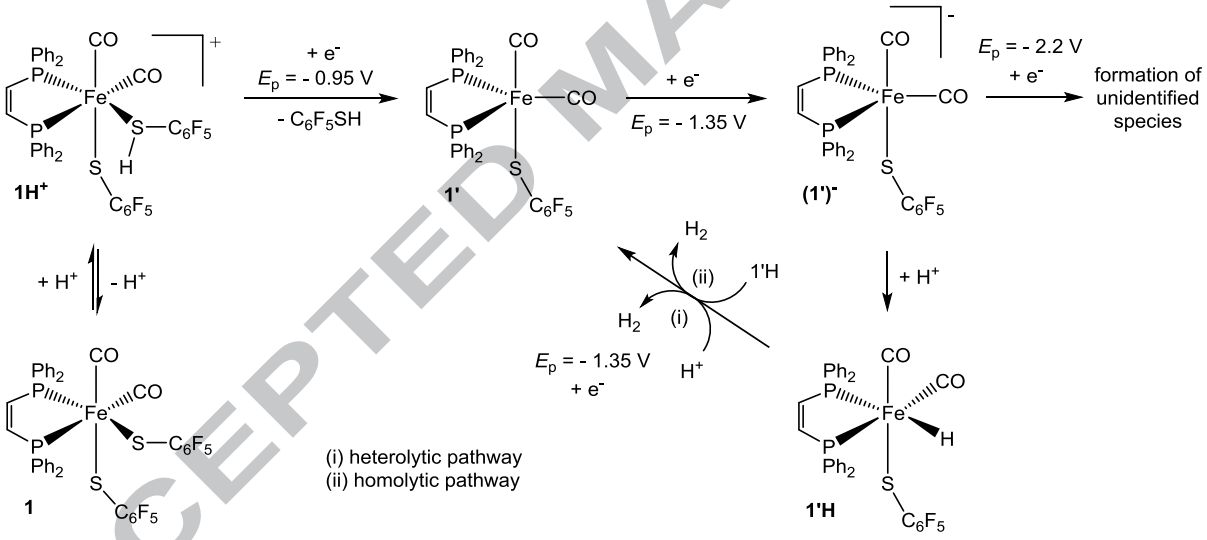

Scheme 4. Speculative catalytic mechanism for the electrocatalytic reduction of protons by $[Fe(CO)_2(\kappa^2\text{-dppv})(\kappa^1\text{-}SC_6F_5)_2]$ (**1**).

Figure 5 shows a plot of catalytic current/non-catalytic current ratio (i_{cat}/i_p) *vs* acid concentration. The i_{cat}/i_p value increases to 46 after addition of 10 equivalents of $HBF_4{\cdot}Et_2O$ for the first catalytic wave, while the ratio approaches 27 for the second wave at similar acid concentrations. The i_{cat}/i_p value of **1** obtained from this study is almost 5-fold greater than that of $[Fe(CO)_2(PMe_3)_2(\kappa^2\text{-}SC_6H_2Cl_2S)]$ (i_{cat}/i_p ~10) [7]. The catalytic activity of **1** is matched only by cobalt complexes $[(dmgBF_2)_2Co(NCMe)_2]$ ($dmgBF^2$ = difluoroboryl-dimethylglyoxime) (i_{cat}/i_p ~30) [19] reported by Peters and $[(P^{Ph}{}_2N^{Ph}{}_2)Co(MeCN)_3]^{2+}$ ($P^{Ph}{}_2N^{Ph}$

= 1,3,6-triphenyl-1-aza-3,6-diphosphacycloheptane) (i_{cat}/i_p ~30) [20] and the nickel complex $[(P^{Ph}{}_2N^{Ph})Ni]^{2+}$ (i_{cat}/i_p 38) [21] reported by DuBois.

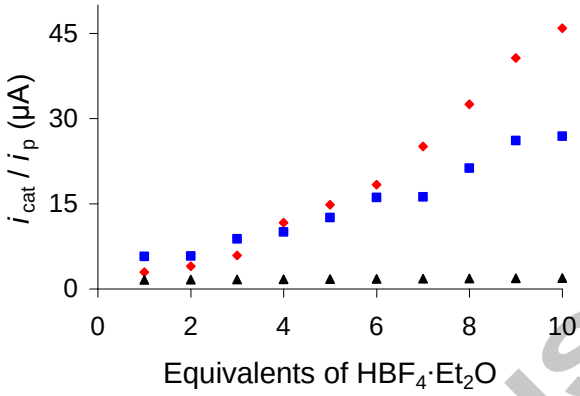

Fig. 5. Dependence of i_{cat}/i_p on $HBF_4{\cdot}Et_2O$ concentration for $[Fe(CO)_2(\kappa^2\text{-dppv})(\kappa^1\text{-}SC_6F_5)_2]$ (**1**) - at potentials of the first (black triangles), second (red diamonds) and third (blue squares) reduction waves (0.5 m*M* solution in acetonitrile, 1-10 equivalents $HBF_4{\cdot}Et_2O$, supporting electrolyte $[NBu_4][PF_6]$, scan rate 0.1 Vs^{-1}, glassy carbon electrode).

CVs of **2** and **3** are relatively complicated as compared to that of **1** probably due to the increasing amount of 'S-*trans*' isomer in solution (Chart 2). The CV of **2** shows an irreversible reduction at E_p = –1.55 V followed by a second reduction at E_p = –2.03 V (Fig. S4a). The reversibility of the second reduction improved at higher scan rates (≥ 0.5 Vs^{-1}). The first oxidation of **2** occurs at E_p = –0.19 V, a *ca.* 1 V negative shift compared to the oxidation potential of **1**, which is followed by two further oxidations at E_p = 0.20 and 0.45 V. Complex **3** undergoes a quasi-reversible reduction at $E_{1/2}$ = –1.49 V followed by two small irreversible reductive features at E_p = –2.05 and –2.27 V (Fig. S5a). It undergoes two irreversible oxidations at E_p = 0.06 and 0.69 V. No significant change was observed when the scan rate was varied.

Both **2** and **3** show similar catalysis in the presence of $HBF_4{\cdot}Et_2O$ but with poorly resolved catalytic waves (Figs. S4b and S5b). Both show three new reduction peaks upon addition of 1 equivalent of $HBF_4{\cdot}Et_2O$ (at E_p = –1.15, –1.45 and –1.95 V for **2**; at E_p = –1.00, –1.40 and –2.00 V for **3**). Akin to **1**, the peak current of the second and third waves increase with the concentration of acid, while that of the first wave remains constant throughout the experiment. Plots of limiting current at the first catalytic wave against concentration of acid for **1**-**3** (Fig. 6) show that the catalytic efficiency of **1** is far better than that of **2** and **3**, as the

limiting current observed for the later two complexes are almost negligible compared to that of **1**. Usually the limiting current (catalytic efficiency) increases as the basicity of the metal centre is increased. The opposite trend observed for this series is probably related to the instability of these complexes in the presence of $HBF_4 \cdot Et_2O$. As discussed in the previous section, loss of a thiol after protonation at sulphur is relatively fast for **2** and **3** as compared to **1**, which also explains the unresolved catalytic currents observed in the CVs of **2** and **3**.

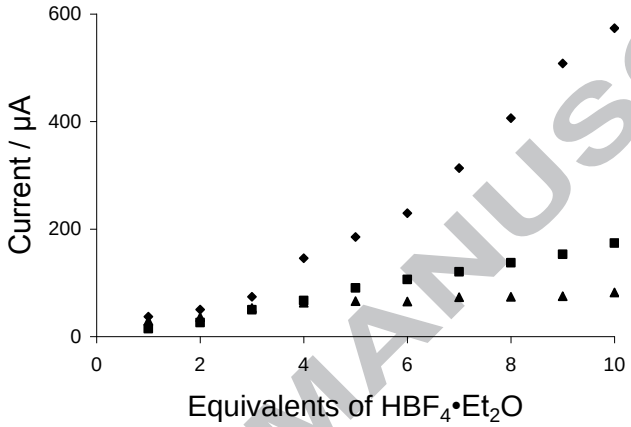

Fig. 6. Plot of catalytic limiting current at potentials of first catalytic wave *vs.* equivalents of $HBF_4 \cdot Et_2O$ added for $[Fe(CO)_2(\kappa^2\text{-dppv})(\kappa^1\text{-}SC_6F_5)_2]$ (**1**) (diamonds), $[Fe(CO)_2(\kappa^2\text{-dppv})(\kappa^1\text{-}SC_6H_5)_2]$ (**2**) (squares) and $[Fe(CO)_2(\kappa^2\text{-dppv})(\kappa^1\text{-}SC_6H_4CH_3\text{-}p)_2]$ (**3**) (triangles).

Conclusions

Mononuclear iron(II) bis(thiolate) complexes **1**-**3** have been synthesized and tested as catalysts for electrocatalytic proton reduction. The crystal structures show that the thiolate ligands adopt an all *cis*-configuration in the solid-state, but exist in both *cis*- and *trans*-configurations in solution. Their redox response is highly sensitive to the nature of thiolate ligand. As expected, complex **1** with electron-withdrawing fluorine substituents, reduces at least negative potential but its oxidation potential is the most positive. Although the redox features in their CVs are quite different from each other, all undergo a quasi-reversible reduction at a relatively mild potential as compared to the corresponding diiron hexacarbonyl [16,22]. All protonate at sulphur upon addition of acid and lose a thiolate ligand as thiol. While all three catalyze proton reduction at mild potentials, the efficiency of **1** is far better than **2** and **3** which we attribute due to the greater stability of **1** in presence of acid.

Electrochemical data supports the hypothesis that a penta-coordinated 17-electron species, $[Fe(CO)_2(\kappa^2\text{-dppv})(\kappa^1\text{-SAr})]$, generated *in situ* by reduction and concomitant loss of a thiolate ligand is the actual catalytic species. Akin to the related iron dithiolate complexes $[Fe(CO)_2(PMe_3)_2(\kappa^2\text{-}SC_6H_2R_2S)]$ reported by Ott and co-workers [9], each shows two catalytic waves involving two oxidation states of iron but the catalytic mechanism of **1**-**3** is significantly different from that of $[Fe(CO)_2(PMe_3)_2(\kappa^2\text{-}SC_6H_2R_2S)]$. In Ott's complexes, the chelating dithiolate ligand remains bound to iron throughout the catalytic cycle. Further, the presence of PMe_3 ligands makes the iron centre more basic as compared to **1**-**3**, and thus penta-coordinated 17-electron species $[Fe(CO)_2(PMe_3)_2(\kappa^1\text{-}SC_6H_2R_2SH)]$ are able to bind protons. This behaviour is not seen for **1**-**3**. Comparison of the catalytic limiting current of **1** with that of $[Fe_2(CO)_6(\mu\text{-}SC_6F_5)_2]$ and $[Fe_2(CO)_4(\mu\text{-}Ph_2PCH_2PPh_2)(\mu\text{-}SC_6F_5)_2]$ [16] (although the catalysis was carried out in different solvent) shows that **1** is a better catalyst than these related dinuclear complexes.

Experimental

General

All reactions were carried out under a dry, oxygen-free nitrogen atmosphere using standard Schlenk techniques. Solvents were stored in alumina columns and dried with anhydrous engineering equipment, such that the water concentration was 5–10 ppm. Metal carbonyls and all other reagents were purchased from various commercial chemical companies and used without further purification. Preparative thin layer chromatography was carried out on 0.25 mm plates prepared from silica gel GHLF (UV254, Analtech). Infrared spectra were recorded using a Nicolet 205 FT-IR or Nicolet 6700 FT-IR spectrometer in a solution cell fitted with calcium fluoride plates, subtraction of the solvent absorptions being achieved by computation. NMR spectra were run on a Bruker AMX400 instrument.

Synthesis of $[Fe(CO)_2(\kappa^2\text{-dppv})(\kappa^1\text{-}SC_6F_5)_2]$ (1)

A toluene (30 mL) solution of $[Fe_2(CO)_6(\mu\text{-}SC_6F_5)_2]$ (100 mg, 0.147 mmol) and dppv (59 mg, 0.149 mmol) was heated at 80-85°C for 24 h. The reaction mixture was cooled to room temperature and filtered. Volatiles were removed under reduced pressure and the residue

redissolved in toluene. A layer of hexane was added to the toluene solution which at room temperature (under nitrogen) gave red crystals of $[Fe(CO)_2(\kappa^2\text{-dppv})(\kappa^1\text{-}SC_6F_5)]$ (**1**) (36 mg, 27%). Data for **1**: IR (νCO, CH_2Cl_2): 2037s, 1993s cm^{-1}. ^1H NMR ($CDCl_3$): δ 8.08 (m, 2H), 7.99 (m, 1H), 7.92 (m, 3H), 7.71 (m, 2H), 7.51 (m, 10H), 7.31 (m, 4H). $^{31}P\{^1H\}$ NMR ($CDCl_3$): major isomer: δ 81.0 (d, J 22 Hz), 58.5 (d, J 22 Hz); minor isomer: δ 77.9 (s). Elemental analysis calc. for $C_{40}H_{22}F_{10}Fe_1O_2P_2S_2$ (found): C 53.00 (51.34), H 2.45 (2.45).

Synthesis of $[Fe(CO)_2(\kappa^2\text{-dppv})(\kappa^1\text{-}SC_6H_5)_2]$ (2)

A xylene (25 mL) solution of $[Fe_2(CO)_6(\mu\text{-}SC_6H_5)_2]$ (150 mg, 0.301 mmol) and dppv (300 mg, 0.757 mmol) was heated to reflux for 1 h. The solvent was removed under reduced pressure and the residue separated by TLC on silica gel. Elution with hexane/CH_2Cl_2 (1:3, v/v) developed two bands on TLC plates. The slower moving band afforded $[Fe(CO)_2(\kappa^2\text{-dppv})(\kappa^1\text{-}SC_6H_5)_2]$ (**2**) (18 mg, 8%) as red crystals after recrystallization from diethyl ether at –30°C, while the contents of the faster moving band were too small for characterization. Data for **2**: IR (νCO, CH_2Cl_2): 2023s, 1978s cm^{-1}. ^1H NMR ($CDCl_3$): δ 8.10 (m, 1H), 8.25 (m, 1H), 7.88 (m, 3H), 7.69 (m, 3H), 7.51-7.33 (m, 18H), 7.03 (m, 4H), 6.90 (m, 2H). $^{31}P\{^1H\}$ NMR ($CDCl_3$): major isomer: δ 80.8 (d, J 23 Hz), 61.1 (d, J 23 Hz); minor isomer: δ 74.1 (s). Elemental analysis calc. for $C_{40}H_{32}FeO_2P_2S_2$ (found): C 66.12 (65.04), H 4.44 (4.51).

Synthesis of $Fe(CO)_2(\kappa^2\text{-dppv})(\kappa^1\text{-}SC_6H_4CH_3\text{-}p)_2$ (3)

A xylene solution (20 mL) of $[Fe_2(CO)_6(\mu\text{-}SC_6H_4CH_3\text{-}p)_2]$ (100 mg, 0.190 mmol) and dppv (189 mg, 0.477 mmol) was heated to reflux for 1 h. The solvent was removed under reduced pressure and the residue chromatographed by TLC on silica gel. Elution with hexane/CH_2Cl_2 (1:3, v/v) developed two bands on TLC plates. The second band afforded $[Fe(CO)_2(\kappa^2\text{-dppv})(\kappa^1\text{-}SC_6H_4CH_3\text{-}p)_2]$ (**3**) (7 mg, 5%) as red crystals after recrystallization from diethyl ether at –30°C, while the contents of the first band were too small for characterization. Data for **3**: IR (νCO, CH_2Cl_2): 2020s, 1975s cm^{-1}. ^1H NMR ($CDCl_3$): major isomer: δ 8.13 (m, 1H), 7.89 (m, 2H), 7.70 (m, 2H), 7.39 (m, 20H), 7.13 (d, J 8 Hz, 2H), 6.90 (d, J 8 Hz, 1H), 6.83 (d, J 8 Hz, 1H), 6.73 (d, J 8 Hz, 1H), 2.34 (s, 6H). $^{31}P\{^1H\}$ NMR ($CDCl_3$): major isomer: δ 80.6 (d, J 21 Hz), 61.0 (d, J 21 Hz); minor isomer: δ 74.4 (s). Elemental analysis calc. for $C_{42}H_{36}FeO_2P_2S_2$ (found): C 66.84 (65.71), H 4.82 (4.91).

Protonation of 1-3

2 equivalents of $HBF_4 \cdot Et_2O$ (0.680 μL) was added to a dichloromethane solution containing 0.005 mmol of the complex to be examined (**1**-**3**) at room temperature. The resulted solution was then transferred into a solution IR cell fitted with calcium fluoride plates and a series of spectra were recorded as a function of time.

Electrochemical studies

Electrochemistry was carried out in deoxygenated acetonitrile solution with 0.05 M $TBAPF_6$ as the supporting electrolyte. The working electrode was a 3 mm diameter glassy carbon electrode that was polished with 0.3 μm alumina slurry prior to each scan. The counter electrode was a Pt wire and the quasi-reference electrode was a silver wire. All CVs were referenced to the Fc^+/Fc redox couple. An Autolab potentiostat (EcoChemie, Netherlands) was used for all electrochemical measurements. Catalysis studies were carried out by adding equivalents of $HBF_4 \cdot Et_2O$ (Sigma-Aldrich).

X-ray crystallography

Single-crystal X-ray diffraction experiment for **1-3** were conducted on a Rigaku Saturn CCD diffractometer (λ = 0.6889 Å) on Station I19 at the Diamond Light Source [23]. Crystallographic data for **1**: red plate, dimensions 0.004 × 0.004 × 0.001 mm^3, monoclinic, space group $P2_1/c$, a = 10.665(6), b = 15.197(9), c = 25.547(16) Å, α = 90, β = 99.200(6), γ = 90°, V = 4087(4) $Å^3$, Z = 4, F(000) 1824, d_{calc} = 1.473 g cm^{-3}, μ = 0.629 mm^{-1}. 23195 reflections were collected, 7138 unique [R(int) = 0.1894]. At convergence, R_1 = 0.0930, wR_2 = 0.2187 [$I > 2.0\sigma(I)$] and R_1 = 0.1338, wR_2 = 0.2545 (all data), for 515 parameters. Crystallographic data for **2**: red block, dimensions 0.04 × 0.04 × 0.04 mm^3, monoclinic, space group $P2_1/n$, a = 11.604 (14), b = 34.74(4), c = 19.35(2) Å, α = 90, β = 106.292(13), γ = 90°, V = 7489(16) $Å^3$, Z = 4, F(000) 3008, d_{calc} = 1.289 g cm^{-3}, μ = 0.632 mm^{-1}. 34061 reflections were collected, 7745 unique [R(int) = 0.0628]. At convergence, R_1 = 0.1452, wR_2 = 0.4340 [$I > 2.0\sigma(I)$] and R_1 = 0.1593, wR_2 = 0.4478 (all data), for 792 parameters. Crystallographic data for **3**: red plate, dimensions 0.04 × 0.04 × 0.001 mm^3, monoclinic, space group $P2_1/n$, a = 12.8737(3), b = 17.3484(4), c = 16.2313(4) Å, α = 90, β = 90.288(2), γ = 90°, V = 3625.02(15)

$Å^3$, Z = 4, F(000) 1568, d_{calc} = 1.383 g cm^{-3}, μ = 0.656 mm^{-1}. 39824 reflections were collected, 10490 unique [R(int) = 0.0620]. At convergence, R_1 = 0.0469, wR_2 = 0.1043 [$I > 2.0\sigma(I)$] and R_1 = 0.0700, wR_2 = 0.1159 (all data), for 444 parameters.

Acknowledgements

We thank the Commonwealth Scholarship Commission for the award of a Commonwealth Scholarship and King's College for postdoctoral funding (SG) and the EPSRC for a postdoctoral fellowship (NH).

Supplementary material

Crystallographic data for the structural analysis of **1**-**3** have been deposited with the Cambridge Crystallographic Data Center, CCDC 1413098 (for **1**), 1413099 (for **2**) and 1413100 (for **3**). Copies of this information may be obtained free of charge from the Director, CCDC, 12 Union Road, Cambridge, CB2 1 EZ, UK (fax: +44-1223-336033; e-mail: deposit@ccdc.cam.ac.uk or www: http://www.ccdc.ac.uk).

References

(1) (a) M.W.W. Adams, E.I. Stiefel, Science 282 (1998) 1842-1843;
(b) R. Cammack, Nature 397 (1999) 214-215;
(c) M. Frey, ChemBioChem 3 (2002) 153-160.

(2) For reviews of this area see: (a) I.P. Georgakaki, L.M. Thomson, E.J. Lyon, M.B. Hall, M.Y. Darensbourg, Coord. Chem. Rev. 238-239 (2003) 255-266;
(b) D.J. Evans, C.J. Pickett, Chem. Soc. Rev. 32 (2003) 268-287;
(c) T.B. Rauchfuss, Inorg. Chem. 43 (2004) 14-26;
(d) L. Sun, B. Åkermark, S. Ott, Coord. Chem. Rev. 249 (2005) 1653-1663;
(e) X. Liu, S.K. Ibrahim, C. Tard, C.J. Pickett, Coord. Chem. Rev. 249 (2005) 1641-1652;
(f) C. Tard, C.J. Pickett, Chem. Rev. 109 (2009) 2245-2274;
(g) J.-F. Capon, F. Gloaguen, P. Schollhammer, J. Talarmin, Coord. Chem. Rev. 249 (2005) 1664-1676.

(3) (a) S. Ghosh, G. Hogarth, K.B. Holt, S.E. Kabir, A. Rahaman, D. Unwin, Chem. Commun. 47 (2011) 11222-11224;

(b) S. Ghosh, G. Hogarth, N. Hollingsworth, K.B. Holt, I. Richards, M.G. Richmond, B.E. Sanchez, D. Unwin, Dalton Trans. 42 (2013) 6775-6792;

(c) F.I. Adam, G. Hogarth, I. Richards, B.E. Sanchez, Dalton Trans. (2007) 2495–2498;

(d) F.I. Adam, G. Hogarth, I. Richards, J. Organomet. Chem. 692 (2007) 3957–3968;

(e) F.I. Adam, G. Hogarth, S.E. Kabir, I. Richards, C. R. Chim. 11 (2008) 890–905.

(4) (a) J.W. Peters, W.N. Lanzilotta, B.J. Lemon, L.C. Seefeldt, Science 282 (1998) 1853-1858;

(b) Y. Nicolet, C. Piras, P. Legrand, C.E. Hatchikian, J.C. Fontecillacamps, Structure 7 (1999) 13-23;

(c) A. Adamska-Venkatesh, S. Roy, J.F. Siebel, T.R. Simmons, M. Fontecave, V. Artero, E. Reijerse, W. Lubitz, J. Am. Chem. Soc. 137 (2015) 12744-12747

(5) C. Sommer, A. Adamska-Venkatesh, K. Pawlak, J.A. Birrell, O. Rüdiger, E. Reijerse, W. Lubitz, J. Am. Chem. Soc. 139 (2017) 1440-1443.

(6) I. Bhugun, D. Lexa, J.-M. Saveánt, J. Am. Chem. Soc. 118 (1996) 3982-3983.

(7) M.J. Rose, H.B. Gray, J.R. Winkler, J. Am. Chem. Soc. 134 (2012) 8310-8313.

(8) V. Artero, M. Fontecave, C. R. Chimie 11 (2008) 926-931.

(9) S. Kaur-Ghumaan, L. Schwartz, R. Lomoth, M. Stein, S. Ott, Angew. Chem. Int. Ed. 49 (2010) 8033-8036.

(10) M. Beyler, S. Ezzaher, M. Karnahl, M.-P. Santoni, R. Lomoth, S. Ott, Chem. Commun. 47 (2011) 11662-11664.

(11) A. Orthaber, M. Karnahl, S. Tschierlei, D. Streich, M. Stein, S. Ott, Dalton Trans. 43 (2014) 4537-4549.

(12) S. Roy, S.K.S. Mazinani, T.L. Groy, L. Gan, P. Tarakeshwar, V. Mujica, A.K. Jones, Inorg. Chem. 53 (2014) 8919-8929.

(13) G.P. Connor, K.J. Mayer, C.S. Tribble, W.R. McNamara, Inorg. Chem. 53 (2014) 5408-5410.

(14) S. Gao, J. Fan, S. Sun, F. Song, X. Peng, Q. Duan, D. Jiang, Q. Liang, Dalton Trans. 41 (2012) 12064-12074.

(15) A. Rana, B. Mondal, P. Sen, S. Dey, A. Dey**,** Inorg. Chem. 56 (2017) 1783-1793.

(16) F. Ridley, S. Ghosh, G. Hogarth, N. Hollingsworth, K.B. Holt, D.G. Unwin, J. Electroanal. Chem. 703 (2013) 14-22.

(17) J.A. De Beer, R.J. Haines, J. Organomet. Chem. 36 (1972) 297-312.

(18) J. Takács, L. Markó, L. Párkányi, J. Organomet. Chem. 361 (1989) 109-116.

(19) X. Hu, B. S. Brunschwig, J. C. Peters, J. Am. Chem. Soc. 129 (2007) 8988-8998.

(20) G.M. Jacobsen, J.Y. Yang, B. Twamley, A.D. Wilson, R.M. Bullock, M. Rakowski-DuBois, D.L. DuBois, Energy Environ. Sci. 1 (2008) 167-174.

(21) M.L. Helm, M.P. Stewart, R.M. Bullock, M. Rakowski-DuBois, D.L. DuBois, Science 333 (2011) 863-866.

(22) D. Chong, I.P. Georgakaki, R. Mejia-Rodriguez, J. Sanabria-Chinchilla, M.P. Soriaga, M.Y. Darensbourg, Dalton Trans. (2003) 4158-4163.

(23) H. Nowell, S.A. Barnett, K.E. Christensen, S.J. Teat, D.R. Allan, J. Synchrotron Rad. 19 (2012) 435-441.

Graphical Abstract

Electrocatalytic proton reduction by $Fe(CO)_2(\kappa^2\text{-dppv})(\kappa^1\text{-SAr})_2$ (dppv = *cis*-1,2-bis(diphenylphosphino)ethylene; Ar = C_6F_5, C_6H_5, $C_6H_4CH_3$-*p*)

Shishir Ghosh*, Nathan Hollingsworth, Mark Warren, Katherine B. Holt, Graeme Hogarth*

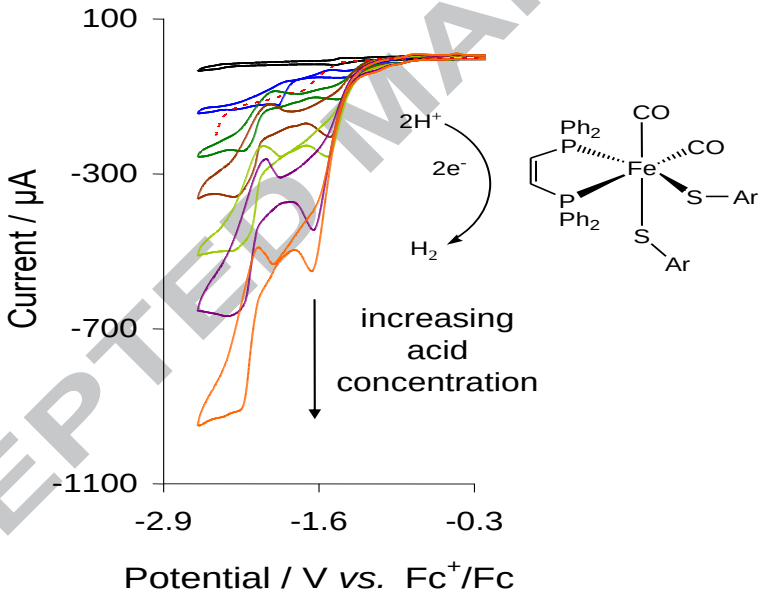

Graphical Abstract synopsis

A series of iron(II) bis(thiolate) complexes of the general formula $[Fe(CO)_2(\kappa^2\text{-dppv})(\kappa^1\text{-SAr})_2]$ have been investigated as electrocatalysts for the reduction of protons to hydrogen.